SIMULATION AND CORRECTION OF TRIANA VIEWED EARTH RADIATION BUDGET WITH ERBE DATA

Patrick Minnis[1], Jianping Huang[2], David R. Doelling[2], Francisco P. J. Valero[3]

[1]Atmospheric Sciences
NASA Langley Research Center
Hampton, Virginia USA

[2]AS&M, Inc.
Hampton, Virginia USA

[3]Atmospheric Research Laboratory
Scripps Institute of Oceanography
La Jolla, CA USA

Proceedings of SPIE 8th International Symposium on Remote Sensing
Toulouse, France
17-21 September 2001

SIMULATION AND CORRECTION OF TRIANA VIEWED EARTH RADIATION BUDGET WITH ERBE DATA

P. Minnis[1], J. Huang[2], D. R. Doelling[2], F. P. J. Valero[3]

[1]Atmospheric Sciences
NASA Langley Research Center
Hampton, Virginia USA

[2]AS&M, Inc.
Hampton, Virginia USA

[3]Atmospheric Research Laboratory
Scripps Institute of Oceanography
La Jolla, CA USA

ABSTRACT

This paper describes the simulation of the earth radiation budget (ERB) as viewed by Triana and the development of correction models for converting Triana-viewed radiances in to a complete ERB. A full range of Triana views and global radiation fields are simulated using data from the Earth Radiation Budget Experiment (ERBE) and analyzed with a set of empirical correction factors specific to the Triana views. The results show that the accuracy of global correction factors to estimate ERB from Triana radiances is a function of the Triana position from Lagrange-1 (L1) or the Sun position. Spectral analysis of the global correction factor indicates that both shortwave (SW) and longwave (LW) parameters undergo seasonal and diurnal cycles that dominate the periodic fluctuations. The diurnal cycle, especially its amplitude, is also strongly dependent on the seasonal cycle. Based on these results, models are developed to correct the radiances for unviewed areas and anisotropic emission and reflection. A preliminary assessment indicates that these correction models can be applied to Triana radiances to produce the most accurate global ERB to date.

1. INTRODUCTION

Triana is designed to continually monitor the sunlit side of the earth and promises to offer new insights into how our planet's climate works as an integrated system. It will be the first Earth-observing satellite in a Lagrange-1 (L1) position at distance of roughly 1.5 million kilometers from the Earth. The L1 point is the location where the Earth's gravitational field equally counters that of the sun. Since the strength of the gravitational attraction determines the orbital period, Triana will orbit the sun at the same rate as the Earth. Triana will be placed in an elliptical Lissajous orbit about L1 and will vary from 4° to 15° about the Earth-sun line. It will continuously measure between 92 and 97% of the Sunlit Earth, never viewing the dark side of the planet. Triana's Earth-viewing instruments consist of the Scripps-EPIC (Earth Polychromatic Imaging Camera), a 10-channel imager, and the Scripps-NISTAR (National Institute of Standards and Technology Absolute Radiometer), a single-pixel 4-channel broadband cavity radiometer[1]. Data from the Scripps-EPIC and Scripps-NISTAR will be used to monitor the

Earth's radiant power and to analyze weather systems and cloud patterns in an entirely new way.

The ERB consists of the balance between absorbed solar radiation and longwave radiation emitted by the Earth's surface and atmosphere. The emitted radiation is measured while the absorbed sunlight is determined as difference between the incident and the observed solar radiation reflected by the Earth system. ERB measurements at the top of the atmosphere (TOA) are fundamental quantities for monitoring the global climate system. These measurements have traditionally been obtained from ERB instruments on polar-orbiting satellites that typically view a region of the earth only twice each day. They cannot provide continuous spatial coverage of the Earth's entire surface at a specific time or provide continuous temporal coverage for a specific location. NISTAR is designed to facilitate determination of the radiation budget for an entire hemisphere every 10 min or less from a single set of 3 measurements. The NISTAR channels measure the total (TOT, 0.2 - 100 μm), shortwave (SW, 0.2 - 4.0 μm), and near-infrared (NIR, 0.7 - 4.0 μm) radiances with an active cavity radiometer and visible (0.3 - 1.0 μm) radiances with a photodiode. Longwave (LW, 4 - 100 μm) radiances are computed by subtracting the SW from the TOT radiances. Each Triana radiance measurement represents the entire Earth view. However, to derive the ERB from these radiances, it is necessary to convert each radiance to a flux and to account for the radiation field of the dark half of the earth. The Earth's surface and atmosphere are anisotropic reflectors and emitters resulting in a relatively complex variation of radiance leaving the Earth as a function of the viewing and illumination conditions. Triana views the Earth from a limited range of angles corresponding to scattering angles between 165° and 176°. Therefore, to convert radiance to flux requires the use of anisotropic directional models (ADM) to account for the emittance and reflectance anisotropies. Additionally, a sliver of the sunlit Earth (missing light) is out of view (replaced by a dark sliver) because the satellite will not be positioned exactly on the Earth-sun line. This missing light must be taken into account for a complete ERB. Finally, no LW measurements are taken at night. Thus, some means is needed to account for the LW fluxes at night. This paper describes the simulation of a Triana-viewed ERB and the development of correction models using data from the Earth Radiation Budget Experiment (ERBE). Section 2 summarizes the ERBE data. Section 3 describes the simulation of the Triana-viewed ERB. Section 4 analyzes and applies the ERB dataset to develop correction models. Conclusions and a discussion of future work are presented in section 5.

2. ERBE DATA

ERBE was a multi-satellite system designed to measure the ERB. ERBE data were collected from three satellites (the Earth Radiation Budget Satellite ERBS, NOAA-9, and NOAA-10)[2]. Each satellite measured broadband SW and LW radiances from cross-track scanners and wide-field-of-view radiometers. The ERBS scanner nominal field of view at nadir was 47 km^2. The ERBS is in a 56^o inclined orbit, which allows it to precess and sample all hours of the day in a 36-day period. NOAA-9 and NOAA-10 were polar orbiters with local equator crossing times of 1420 and 0730. Bidirectional reflectance and limb-darkening models[3,4] were used to convert radiances into fluxes[5,6] for 4 identified scene types; clear, partly cloudy, mostly cloudy, and overcast. The first three scene types were further subcategorized for the surface type: ocean, land, desert, snow, and coast. NOAA-9 and NOAA-10 provided global coverage, while ERBS sampled between 67.5° north and south latitudes. Instruments on the three satellites began acquiring data in November 1984, February 1985, and October 1986, respectively. The NOAA-9 scanner ceased operations on January 20, 1987 and the NOAA-10 scanner on May 22, 1989. The ERBS scanner ceased operations on February 28, 1990. This combination of multiple satellite is used to produce a Triana-viewed

ERB. In this study, we use 4 years (Jan. 1985 to Dec. 1988) of ERBE S-9 data to develop a simulated Triana dataset. The ERBE S-9 data consist of hourly estimates of SW albedo and OLR on a 2.5° global grid. Information about the fraction of each scene type and its OLR and albedo is also available for each estimate. More information on the available ERBE products can be found at the Langley DAAC Information Management System.

3. SIMULATION OF TRIANA-VIEWED EARTH RADIATION BUDGET

The simulation for the Triana-viewed ERB can be divided into two parts: SW and LW. The desired SW parameters are: Triana global mean albedo, reflectance, and the bidirectional and missing light albedo correction factors. The desired LW parameters are global mean LW radiance, OLR flux, limb-darkening factor and nighttime OLR correction factor. The objective of this section is to derive these parameters from the ERBE data to measure the effect of the Triana position on the estimation of ERB. Most points on the sunlit side of the Earth will be viewed simultaneously from sunrise to sunset. The first step in the simulation is to temporally interpolate ERBE fluxes to the Triana observation times using the ERBE time and space averaging techniques[7]. The second step is to make global averages taking the unviewed portions of the earth into consideration.

3.1 Short wave

For any given Triana observation time, the ERBE albedo for a given 2.5° grid box can be expressed as the weighted average of the product of the observed albedo and the ratio of the normalized angular distribution models (ADM) function from the Triana time and ERBE observation time:

$$\alpha_{erbe}(\mu_T) = w_1 \sum_{i=1}^{4} \alpha_{erbe}(\mu_1)\, \delta_i(\mu_T) / \delta_i(\mu_1) \; + \; w_2 \sum_{i=1}^{4} \alpha_{erbe}(\mu_2)\, \delta_i(\mu_T) / \delta_i(\mu_2) \qquad (1)$$

where

$$w_1 = (t_2 - t_T) / (t_2 - t_1),\ w_2 = (t_T - t_1) / (t_2 - t_1)$$

t_T is the Triana time, t_1, t_2 are the two closest ERBE observation times, μ_T, μ_1 and μ_2 are the cosines of the solar zenith angle for corresponding times, and δ_i is the ratio of the normalized directional albedo function for the four ERBE cloud classifications. Assuming Triana has perfect spatial sampling, the regional Triana albedo is equal to the ERBE albedo. The regional Triana albedos are then given by:

$$\alpha_{Triana}(\mu_T) = \alpha_{erbe}(\mu_T) \qquad (2)$$

Using the same ERBE scene identifications, the reflectance based on Triana viewing geometry for a given albedo is:

$$R_{triana}(\mu_T, vz_T, ra_T, scene_T) = \alpha_{erbe}(\mu_T)\, \chi\, (\mu_T, vz_T, ra_T, scene_T) \qquad (3)$$

where χ is the bidirectional reflectance factor, vz_T the Triana viewing zenith angle, and ra_T the Triana relative azimuth angle. Triana will view the Earth from near-backscatter conditions so that ra_T will always be greater than 165°. Due to the Triana orbit, 2% - 8 % of the sunlit Earth will out of view. Figure 1 shows an example of Triana-viewed albedo assuming an offset position of 15° East from L1. The dark sliver on the left-hand side of the figure corresponds to the unilluminated portion of the Triana-viewed half disc. A corresponding sunlit sliver behind the right side of the disc out of the field of view referred to

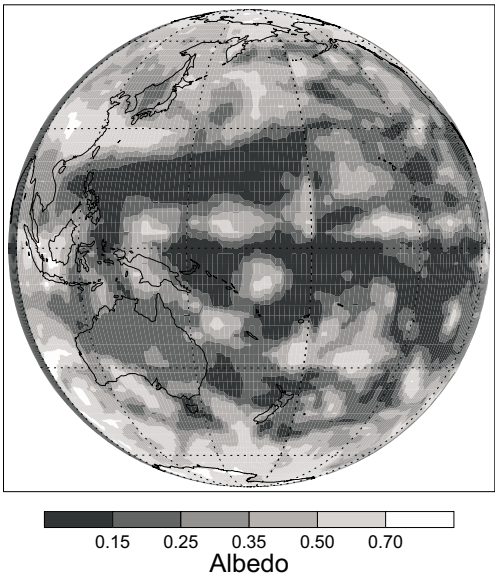

Fig. 1. Simulated Triana-viewed albedo from ERBE data for March 21, 1986 at 15^{o} east from L1.

as the missing light area. This missing light area must be estimated to compute the global mean albedo. The global mean Triana albedo and reflectance are derived from the sunlit regions as follows:

$$\overline{\alpha}_{\text{triana}}(T_d, T_g) = \sum_{earth}^{vz<90} \alpha_{\text{triana}}(\mu_i)\ \mu_i \cos(lat_i) \Big/ \sum_{earth}^{vz<90} \mu_i \cos(lat_i), \tag{4}$$

$$\overline{R}_{\text{triana}}(T_d, T_g) = \sum_{earth}^{vz<90} R_{triana}(\mu_T, vz_T, ra_T, scene_T)\ \mu_i \cos(lat_i) \Big/ \sum_{earth}^{vz<90} \mu_i \cos(lat_i). \tag{5}$$

T_d and T_g are the calendar day and UTC, respectively, and $\mu_i \cos(\text{lat}_i)$ accounts for the solar insolation and area weighting of the regions. The respective global bidirectional and missing light albedo correction factors, therefore, are given by

$$\overline{\chi}_{\text{triana}}(T_d, T_g) = \overline{R}_{\text{triana}}(T_d, T_g) \Big/ \overline{\alpha}_{\text{triana}}(T_d, T_g) \tag{6}$$

and

$$\overline{\alpha}_{\text{Factor}}(T_d, T_g) = \overline{\alpha}_{\text{erbe}}(T_d, T_g) \Big/ \overline{\alpha}_{\text{triana}}(T_d, T_g). \tag{7}$$

Due to the earth's differing surface types and variations in cloud conditions, $\overline{\chi}_{\text{triana}}$ and $\overline{\alpha}_{\text{Factor}}$ depend on the sub-satellite position. This Triana nadir point from L1 (solar nadir point) is defined as the "L1 offset position" or LO and is described in polar coordinates by angle from north and angular distance from L1. Figure 2 shows the monthly means of global reflectance, albedo, bidirectional factor, and missing light albedo correction factor as a function of LO at 0000 UTC, March 1986. The values of reflectance (Fig. 2a), albedo (Fig. 2b), and $\overline{\chi}_{\text{triana}}$ (Fig. 2c) decrease monotonically with distance from L1. But the patterns of missing light albedo factor (Fig. 2d) are just the opposite. The bidirectional factor is greatest at the L1 position

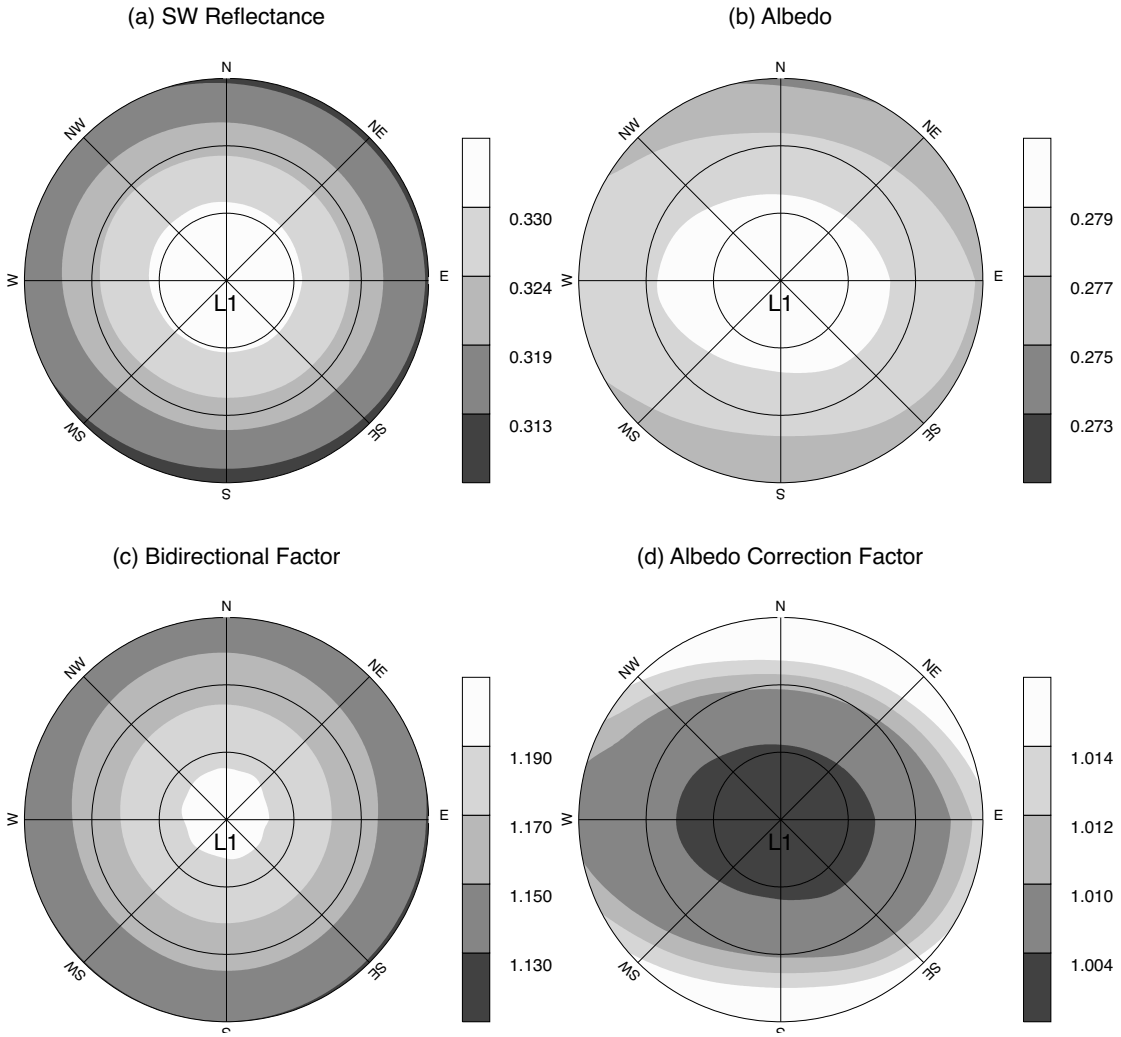

Fig. 2. Monthly mean global Triana short-wave parameters as a function of LO at 0000 UTC for March 1986.

because it is the point at which no shadows are observed. The fraction of shadowed areas increases with distance from L1. The maximum missing light albedo factor appears to occur at 15° N or 15° S off L1 because of the highly reflective polar regions and the large unviewed sliver of the sunlit disc. At the equinox, both poles are equally sunlit, however, observing only one pole is apparently not sufficient to compensate for the unviewed polar region. Seasonal variations in $\overline{\alpha}_{\text{Factor}}$ (Fig. 3) are substantial with the greatest changes evident for the larger L1 offset positions. The seasonal changes arise from variations in surface albedo and clouds. The asymmetry in $\overline{\alpha}_{\text{Factor}}$ for the two hemispheres is caused by the large seasonal variation in snow cover in the Northern Hemisphere as compared to the relatively minor variation in the Southern Hemisphere. However, moving LO away from the sunlit pole during the solstice generates a large correction factor. In addition to snow and ice, seasonal changes in cloudiness and vegetation will also affect the missing light albedo correction factor. The parameters shown in Figs. 2 and 3 also vary with sub-satellite point or UTC. Thus, the values of $\overline{\chi}_{\text{triana}}$ and $\overline{\alpha}_{\text{Factor}}$ will vary with the L1 offset position, the time of day, and the month or day.

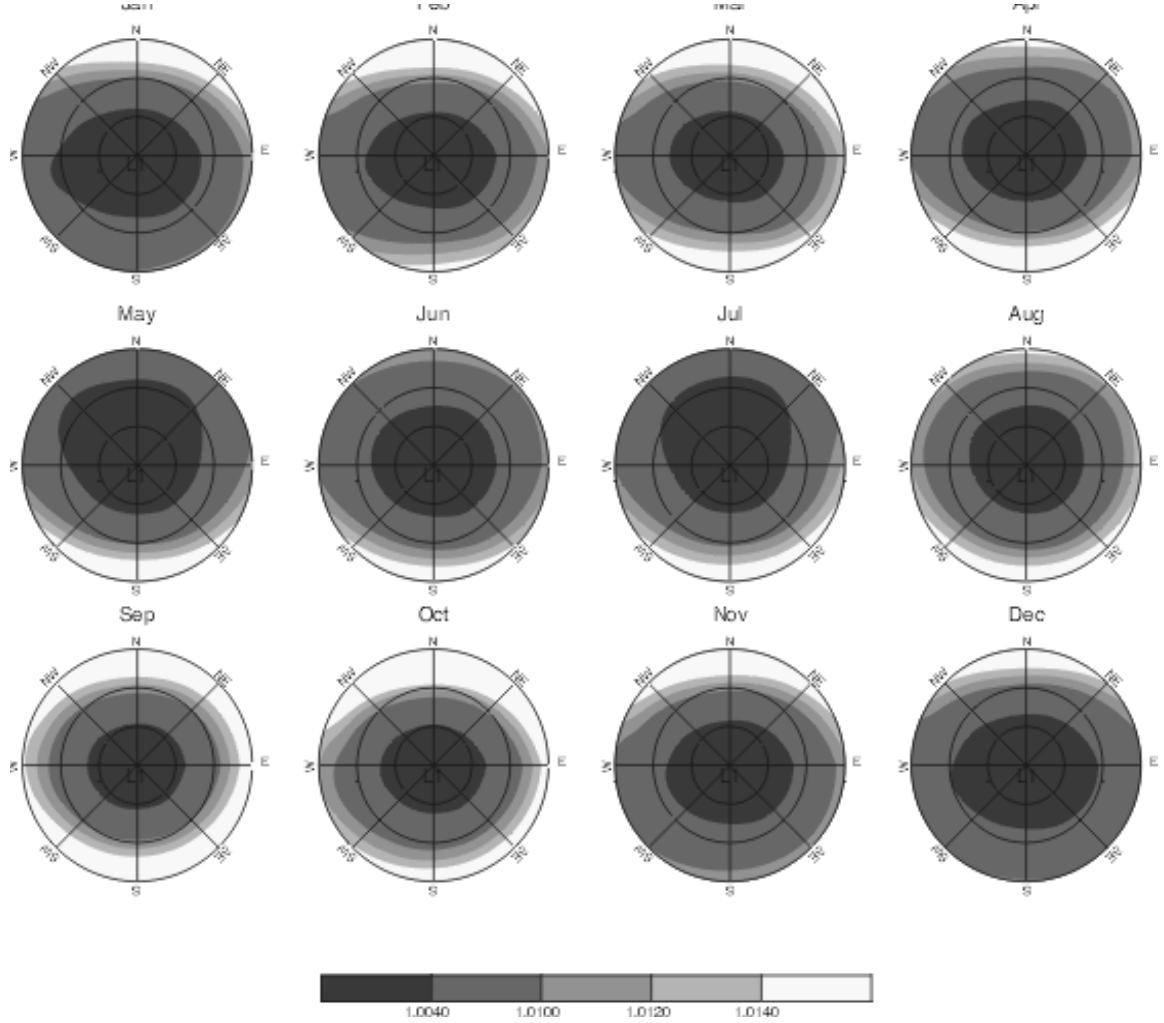

Fig. 3. Seasonal variation of monthly mean global missing light albedo correction factor as a function of LO at 0000 UTC for 1986.

3.2 Long Wave

Similar to the relationship between Triana and ERBE in the SW, the regional Triana OLR can be derived from the ERBE OLR by linearly interpolating from the nearest preceding and following ERBE-estimated fluxes as follows.

$$OLR_{triana}(t_T) = OLR_{erbe}(t_T). \tag{8}$$

The regional LW radiance viewed by Triana

$$RAD_{triana}(vz_T, scene_T) = \alpha_{erbe}(\mu_T)\ \gamma(\ vz_T, scene_T) \tag{9}$$

depends on the limb-darkening factor γ, a parameter that is governed by the viewing zenith angle and the atmospheric and cloud conditions[4]. The respective global mean Triana OLR, LW radiance, and nighttime OLR correction factors are as follows.

$$\overline{OLR}_{triana}(T_d, T_g) = \sum_{earth}^{vz<90} OLR_{triana}(t_T)\cos(lat_i) \Big/ \sum_{earth}^{vz<90} \cos(lat_i) \tag{10}$$

$$\overline{RAD}_{triana}(T_d, T_g) = \sum_{earth}^{vz<90} RAD_{triana}(vz_T, scene_T)\cos(lat_i) \,/\, \sum_{earth}^{vz<90} \cos(lat_i), \tag{11}$$

and

$$\overline{OLR}_{Factor}(T_d, T_g) = \sum_{earth} OLR_{erbe}(t_T)\cos(lat_i) \,/\, \overline{OLR}_{triana}(T_d, T_g). \tag{12}$$

The global limb-darkening factor is

$$\overline{\gamma}_{\text{triana}}(T_d, T_g) = \overline{RAD}_{\text{triana}}(T_d, T_g) \,/\, \overline{OLR}_{\text{triana}}(T_d, T_g). \tag{13}$$

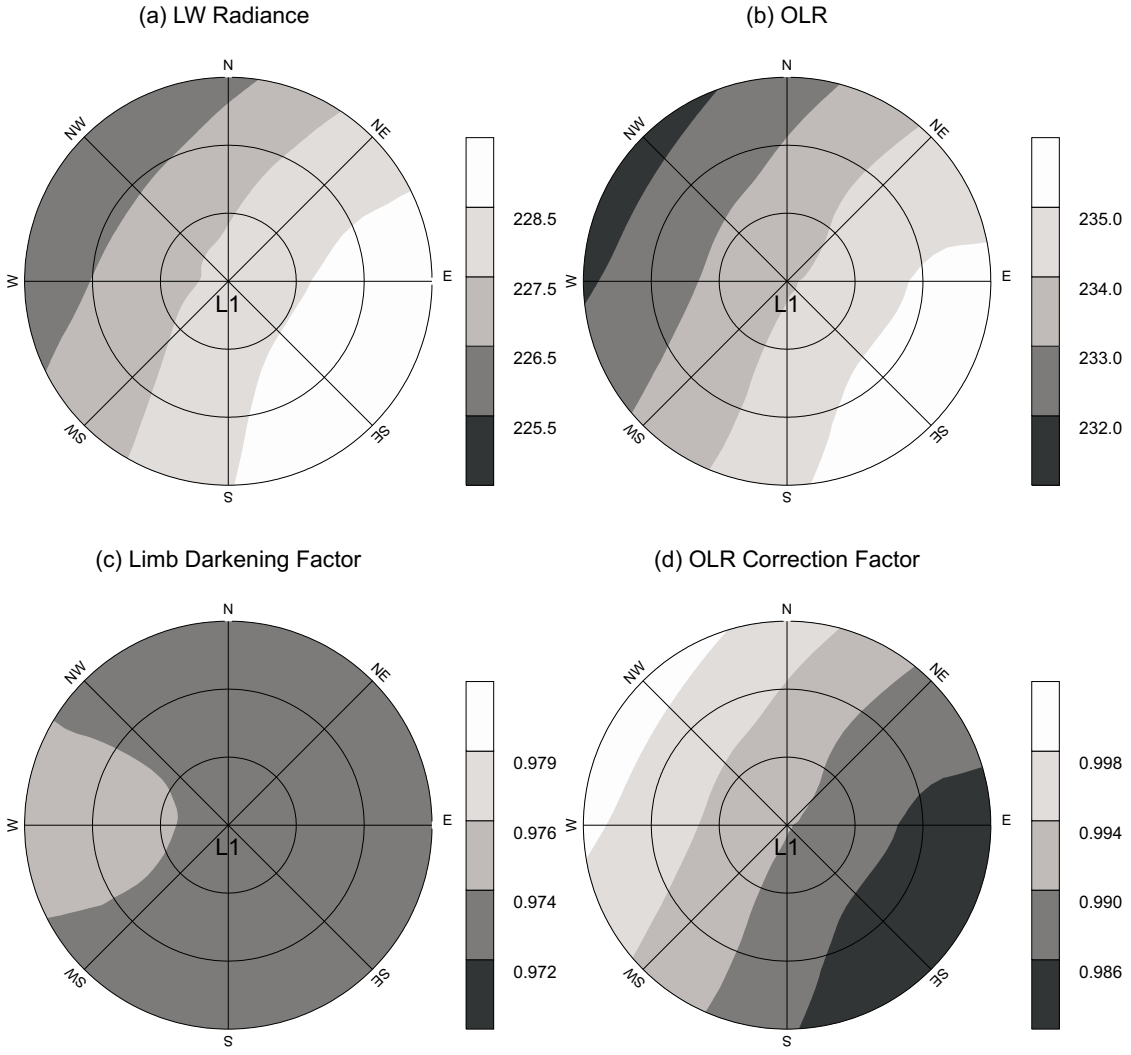

Fig.4. Monthly mean global Triana long-wave parameters as a function of LO at 0000UTC for March 1986.

Figure 4 shows the monthly mean global radiance, OLR, limb-darkening factor, and nighttime OLR correction factor as functions of the L1 offset position at 0000 UTC for March 1986. The patterns of radiance (Fig. 4a) and OLR (Fig. 4b) are very different from that for SW reflectance (Fig. 2a), which is more symmetrical around the L1 point. The highest values of

OLR (~235.5 Wm^{-2}), observed when LO is southeast of L1, decrease gradually towards the northwest to values of ~231.5 Wm^{-2}. In the latter position, the observation is slightly biased to morning views and includes less land. In the southeastern position, the observation is biased to afternoon views and includes more of the Asian land mass. Over land, the clear-sky OLR is typically greater during the afternoon than during the morning. Although the limb-darkening factor varies from 0.973 to 0.975 in Fig. 4c, it is more variable for other views and seasons. The OLR nighttime correction factor (Fig. 4d) shows that Triana-viewed hemispherical OLR is 1.64% greater than the global ERBE OLR at the southeast point where LO = 15°. The seasonal variation (Fig. 5) shows a larger variation with LO than the albedo correction factor shown in Fig. 3, however, the change in value over the full range of LO is much less than the albedo correction factor. The OLR factor is based more on convective high cloud coverage and diurnally varying hot desert surface temperatures. Generally, $\overline{OLR}_{Factor}$ is less than unity because daytime scenes usually emit more radiation than nocturnal ones. Figure 5 demonstrates that, sometimes, the colder hemisphere is viewed during the daytime.

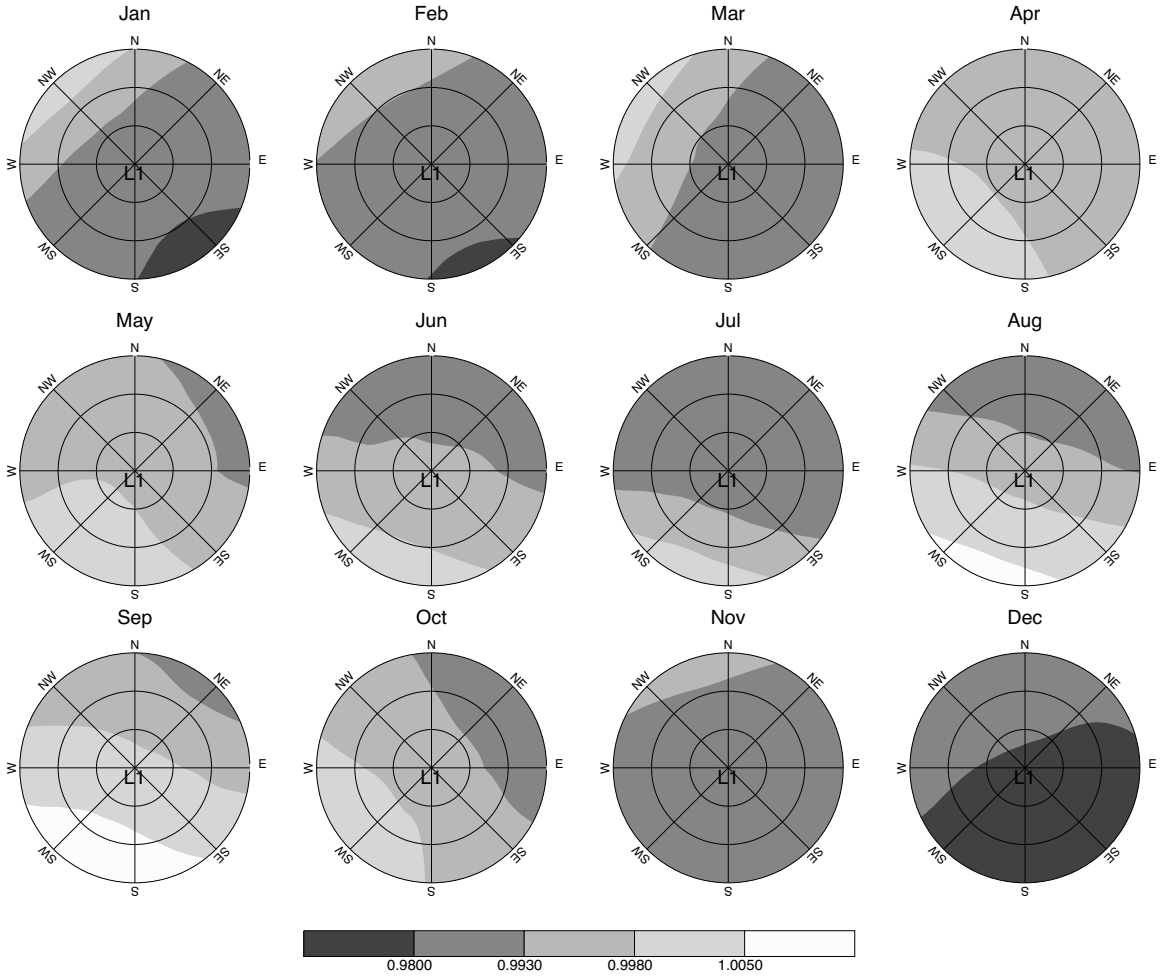

Fig. 5. Seasonal variation of monthly mean global nighttime OLR correction factor as a function of LO at 0000 UTC for 1986.

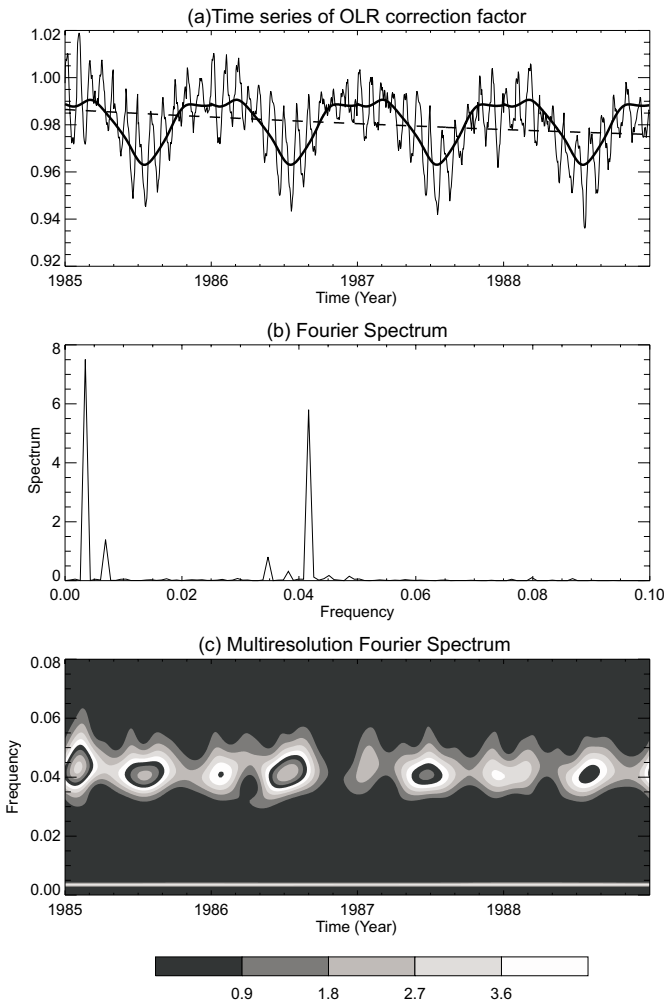

Fig. 6. Time series analysis of simulated monthly-hourly nighttime OLR correction factor at 15^{o} North from L1 for: (a) the original simulated time series (solid line), seasonal cycle (thick solid line) and its long-term trend calculated by a 2-degree polynomial (dash line); (b) Fourier spectrum; (c) multi-resolution Fourier spectrum.

4. DEVELOPMENT OF CORRECTION MODELS

The correction models that will be applied to Triana measurements are developed using more than 4 years (1 Jan., 1985 - 31 Jan, 1989) of daily ERBE data used in equations (1)-(13) to provide simulated Triana measurements for the various L1 offset positions and UTC hours. The following steps are applied to those simulated data sets to obtain data appropriate for time series analysis. First, the daily-hourly data are averaged to create a monthly-hourly dataset. A second-degree polynomial is fitted to those time series using a least squares method to remove the underlying trend. The detrended monthly-hourly time series is then used for analysis. An example of a time series analysis of the OLR correction factor at LO = 15° N (Fig. 6a) reveals a secular downward trend from 1985 to 1988 (long dashed line). A composite average seasonal cycle created by linearly averaging the four annual cycles from 1985 to 1988 is also shown in Fig. 6a (thick solid line). Because of the short length of the data sample, the resulting composite average still retains some fluctuations and fails to produce a smooth seasonal curve. To rectify this sampling deficiency, a low-pass filter technique is applied to filter out the diurnal cycle. Figure 6b shows the Fourier spectrum of the time series shown in Fig. 6a. The result is basically a red spectrum with two

major distinct peaks around frequency 0.0035 (seasonal cycle) and 0.042 (diurnal cycle) indicating that seasonal and diurnal are the two fundamental oscillation frequencies. However, the Fourier spectrum shows no explicit information regarding their temporal locality[8]. Figure 6c shows the multi-resolution Fourier spectra in the frequency and time domain. It confirms that the OLR correction factor has two dominant regimes of periodic fluctuation. On the annual scale, a narrow horizontal bar near the bottom represents the seasonal cycle. However, the diurnal cycle shows the periodic waveform in the time domain. This reveals that diurnal cycle is also strongly modulated by the seasonal cycle, especially its amplitude

Based on the results in Fig. 6, the correction model should include the long-term trend, the seasonal cycle, and the seasonally modulated diurnal cycle. For any time and position, the general correction model can be written as:

$$Y(T_d, T_g, \phi,\theta) = C_0(\phi,\theta) + C_1(\phi,\theta)*T_d + C_2(\phi,\theta)*T_d^2 + C_3(\phi,\theta)*\cos(2\pi f_d T_d) + C_4(\phi,\theta)*\cos(2\pi f_g T_g) + C_5(\phi,\theta)*\cos(2\pi f_d T_d)*\cos(2\pi f_g T_g) \quad (14)$$

where and ϕ the angle from North (in degrees), θ is the distance from L1 (in degrees), and f_d and f_g are the frequencies of the seasonal and diurnal cycles, respectively. The last term in equation (14) represents the effect of modulation. The coefficients, ($C_i(\phi,\theta)$, I=0,…5) were computed using a least squares multiple regression fit for each position. These models can be used to predict the hourly correction factors for any given time (T_d, T_g) and position (ϕ, θ). Three years (Jan. 1985 to Dec. 1987) of simulated data are used as the historical dataset to determine the regression coefficients. The resulting coefficients were used to predict the factors for 1988 and then compared with the simulated data. Examples of the predicted nighttime OLR correction factors at 4 maximum LOs are shown in Fig. 7. The predicted (dashed line) and simulated (solid line) OLR correction factor values are in good agreement except for Northern Hemisphere summer. Preliminary results indicate that the correction model is capable of resolving the global correction factor.

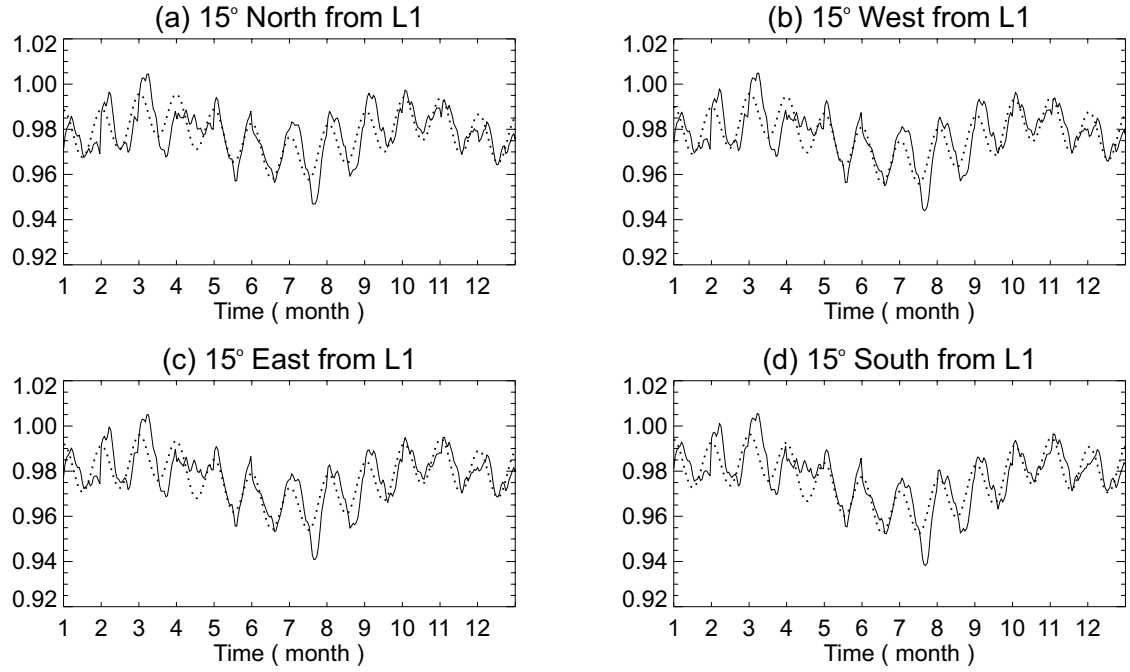

Fig. 7. Predicted (dashed line) and simulated 1988 night OLR correction factors (solid line) for :
(a) 15° north from L1; (b) 15° west from L1; (c) 15° east from L1; (d) 15° South from L1.

5. CONCLUSIONS AND DISCUSSION

This paper provides a basic framework for and some examples of the simulation of Triana-viewed ERB. The simulated ERB based on 4 years of ERBE data have been used to develop of correction models to convert Triana-viewed whole disc radiances into values of global albedo and OLR. The simulation results show that the accuracy of the Triana-viewed ERB depends on the sub-satellite offset position from L1. Time series analysis indicates that the long-term trend, diurnal and seasonal variations are also significant for all the correction factors. The preliminary prediction results indicate that these correction models can be used to produce the most accurate global ERB to date. However, the correction models are purely statistical and it is not possible to distinguish between physical and random relationships in the data. Also, the models may be biased by the sampling patterns of the ERBE satellites. For example, the NOAA-9 and ERBS were used to produce the first 2 years of ERBE data while ERBS and NOAA-10 were used for the last 2 years. The NOAA-9 is an afternoon orbiter while the NOAA-10 has a morning Equatorial crossing time. These two different satellite combinations can produce diurnal sampling biases. To improve on the ERBE sampling, 3 hourly geostationary data will be used to fill the gaps between the ERBE measurements. Further studies will use combinations of ERBS and ISCCP (International Satellite Cloud Climatology Project) datasets to simulate the ERB as measured by Triana. The correction factors developed from each of these datasets will be used for the initial analyses of the Triana NISTAR radiances. A more advanced approach using cloud information from the EPIC is also under development to explicitly account for physical variations in the scene that are not taken into account with the purely empirical method used here. In the meantime, the technique developed here will provide a highly reliable method for monitoring the global radiation balance from Triana.

ACKNOWLEDGMENTS

Special thanks to Kirk Ayers and Michele Nordeen for their help and useful comments. This research was supported by the NASA Triana project.

REFERENCES

1. Valero,F.P.J., J. Herman, P. Minnis, W.D. Collins, R.Sadourny, W. Wiscombe, D.Lubin, and K. Ogilvie, "Triana – a Deep Space Earth and Solar Observatory," NASA background report, (http://triana.gsfc.nasa.gov/home), 1999.
2. B.R. Barkstrom, E. F. Harrison, G. L. Smith, "Results from the Earth Radiation Budget Experiment (ERBE)," *Adv. Space Res.*, **9**, pp. 775 – 782, 1989.
3. J. T. Suttles, R. N. Green, et. al., "Angular radiation models for Earth-atmosphere system: Volume 1 - Shortwave radiation," *NASA RP 1184*, *Vol. I*, 1988.
4. J.T. Suttles, R. N. Green, et al., "Angular radiation models for the Earth-atmosphere systems: Volume II: Longwave radiation," *NASA RP 1184*, Vol. II, 1989.
5. G. L. Smith, R. N. Green, et al., "Inversion methods for satellite studies of the Earth's Radiation Budget: Development of algorithms for the ERBE Mission," *Rev. Geophysics*, **24**, pp. 407 – 421, 1986.
6. B. A. Wielicki and R. N. Green, "Scene identification for ERBE radiative flux retrieval," *J. Appl. Meteorol.*, **28**, pp. 1133 – 1146, 1989.
7. D. F. Young, P. Minnis, D. R. Doelling, G. G. Gibson and T. Wong, "Temporal interpolation methods for the Clouds and the Earth's Radiant Energy System (CERES) Experiment," *J Appl. Meteorol ,* **37**, 572-590, 1998.
8. J. Huang, K. Higuchi and N. B. A. Trivett, "Multi-resolution Fourier transform and its application to analysis of CO_2 fluctuation over Alert," *J. Meteorol. Soc. Japan*, **75**, pp. 701-715, 1997.